Energy 174 (2019) 972–984

Contents lists available at ScienceDirect

Energy

journal homepage: www.elsevier.com/locate/energy

Experimental and theoretical investigation on a radiative flat heat pipe heat exchanger

Sulaiman Almahmoud [a], Hussam Jouhara [a, *]

[a] College of Engineering, Design and Physical Sciences, Brunel University London, Uxbridge, London, UB8 3FG, UK

ARTICLE INFO

Article history:
Received 31 December 2018
Received in revised form
2 March 2019
Accepted 6 March 2019
Available online 9 March 2019

Keywords:
Heat pipe
Radiation
Heat exchanger
Waste heat recovery

ABSTRACT

Large amounts of heat are rejected by hot steel when it is cooling during the manufacturing process. In an earlier investigation a flat heat pipe (FHP) was constructed and tested in a factory for recovering this heat loss from steel wires by radiation and convection. In this paper, the performance of the FHP was examined by testing it at different configurations. In parallel a theoretical study was conducted. The FHP consisted of 14 stainless steel tubes connected by a bottom collector and a shell and tube condenser top header. The heat transfer area was increased by attaching a stainless steel at the back of the tubes. The effect of the back panel on heat recovery was examined by testing the FHP with the back panel and without it. In addition, the effects of the emissivity and absorptivity of the FHP surface on the thermal performance were investigated by testing the FHP both painted with high temperature black paint and with it unpainted. A theoretical modelling tool based on thermal network modelling was built. The theoretical prediction of the thermal performance of the FHP represented by the amount of heat recovery was compared with the experimental findings. The results of the FHP thermal performance were compared for four cases. The results indicated that heat recovery was greatly increased by painting the surface with thermal black paint. Furthermore, the back panel has a significant influence on the magnitude of heat recovery.

1. Introduction

Environment protection has become one of the most concerning problems in the 21st century. Increasing demand on energy resulted in more interest on renewable and sustainable energy technologies and applications [1,2]. However, fossil fuel is still on demand for large energy consuming applications such as industrial applications and manufacturing processes. Steel industry is one of the largest energy consumers in industry sectors. Many steel companies are interested in installing waste heat recovery solutions to utilise the lost heat again in the processes or in other applications [3]. Waste heat recovery technologies in the steel industry contribute to reducing power consumption and the carbon foot print of the process and increasing the energy efficiency of the manufacturing processes. Heat recovery sources in steel industry can be solid product streams such as slags, or hot exhaust gases. The contamination and fouling in the exhaust gases can be challenging for the heat recovery technologies. Exhaust gases are mainly rejected from coke ovens, blast furnaces, oxygen furnaces, and electric arc furnaces [4]. The majority of research on waste heat recovery in the steel industry is focused on waste heat recovery from molten slag utilising fluidized bed heat exchangers [5]. *Liu* et al. have presented and studied a gravity bed waste heat boiler to recover the heat from slag particles [6]. The research investigated the effect of the slag particles diameter on the heat recovery efficiency. *Trashorras* et al. [7] studied the performance of a heat recuperator for waste heat recovery from steel slag. The CFD modelling conducted in the study showed that the heat recuperator can recover up-to 23.2 MW of heat. *Du* et al. presented a novel system to recover the heat from cement rotary kilns by radiation and forced convection from surface of the kiln and hot air flow [8]. The results indicated that the heat recovery system had an important role in controlling the temperature of the shell of the kiln. *Yin* et al. [9] investigated the optimum operating conditions on a heat pipe heat exchanger for waste heat recovery in slag cooling process. The investigation determined the optimum waste and water flow rate corresponding with the highest effectiveness of the system. The effect of cleaning the HPHE from fouling on the thermal performance of the HPHE was also investigated.

* Corresponding author.
E-mail address: hussam.jouhara@brunel.ac.uk (H. Jouhara).

https://doi.org/10.1016/j.energy.2019.03.027

Nomenclature

Symbol

A	Surface area (m^2)
C_p	Specific heat (J/kg.K)
C_{sf}	constant, determined from experimental data
D	Diameter (m)
E	Emitted heat per surface area (W/m^2)
F	View factor
F_{12}	View factor between the heaters plate and external surface of the FHP
F_{13}	View factor between the heaters plate and surrounding
F_{21}	View factor between external surface of the FHP and the heaters plate
F_{23}	View factor between external surface of the FHP and surrounding
g	Gravitational acceleration (m/s^2)
h	Heat transfer Coefficient (W/m^2. K)
h_{fg}	Latent heat of vaporisation (J/kg)
J	Radiosity (W/m^2)
k	Thermal conductivity of liquid (W/m. K)
l	Length (m)
$\dot{m}$	mass flow rate (kg/s)
N	number of pipes
Nu	Nusselt number
Pr	Prandtl number
Q	Heat transfer rate (W)
R	Thermal resistance (K/W)
Re	Reynolds number
T	Temperature (K)

Greek Symbols

μ	Dynamic viscosity (kg/m.s)
ρ	Density (kg/m^3)
σ	Surface tension (N/m)
σ_0	Stefan–Boltzmann constant which is equal to 5.67×10^{-8} $W/(m^2.\ K^4)$
ε	Radiation emissivity

Subscripts

c	Condenser section
ci	Corresponds to inner wall of condenser
co	Corresponds to outer wall of condenser
$cold$	Cooling fluid
$cold,\ in$	Cooling fluid inlet
$cold,\ out$	Cooling fluid outlet
$Cond,\ e$	Evaporator wall conduction
$Cond,\ c$	Condenser wall conduction
ei	Corresponds to inner wall of evaporator
eo	Corresponds to outer wall of evaporator
f	Factor for heat transfer in forced convection
FHP	Corresponds to Flat Heat Pipe
H	Heat source, heaters
l	Liquid
rad	radiation
$surr$	surroundings
v	Vapour

Superscripts

n	experimental constant that depends on fluid

A heat pipe heat exchanger (HPHE) generally consists of multiple heat pipes where each heat pipe acts as an individual heat exchanger. A heat pipe consists of an evacuated tube charged partially with a working fluid as shown in Fig. 1. The heat pipe can transport large amounts of heat for long distances passively and without having any moving parts. This is achieved by utilising two-phase heat transfer by the working fluid in the heat pipe. When the heat pipe is exposed to a high temperature source at his end, the working fluid vaporises and flows towards the condenser at the other end of the heat pipe where it condenses and rejects the heat to the low temperature heat sink. The condensate flows back to evaporator section and the operating cycle is repeated. The condensate can return back to the evaporator by the effect of capillary force when the heat pipe is provided with a wick structure, or by the effect of the gravity force. The gravity assisted heat pipe is also known as thermosyphons [10].

Heat pipes heat exchangers have proven their advantages over conventional heat exchangers in many applications such as waste heat recovery, waste treatment, and solar applications [12]. The advantages of heat pipe heat exchangers include their size and cost reduction, ease of maintenance, uniform wall temperatures and the capability of transporting large heat fluxes. It is also a passive heat transfer device. *Jouhara* et al. has investigated a novel wraparound heat pipe heat exchanger for heat recovery in air handling units [13]. The heat pipe heat exchanger achieved an effectiveness of 30% and the pay-back period of the system was less than two months [14]. *Delpech* et al. [15] investigated the application of HPHE in enhancing the energy efficiency in the ceramic industry. The effect of the HPHE on the kiln was conducted by numerical modelling. It was concluded that utilising the HPHE in waste heat recovery in the kiln will results in significant saving of energy cost. *Delpech* et al. [16] Investigated experimentally a radiative heat pipe in a lab-scale kiln for waste heat recovery by radiation in ceramic industry. The radiative heat pipe was tested at different heaters temperature which were used to simulate the hot ceramic and at difference water flow rate. It was noted that the radiant heat recovery is dominant over natural convection heat recovery at heaters temperature above 300 °C. Heat pipes cannot only be in cylindrical shell case design, but also they can be in a flat shape or a flat evaporator with a cylindrical condenser. A flat heat pipe (FHP) utilises the features of heat pipes and additionally it maximises the heat transfer area and transforms a flat surface into an isothermal surface. Flat heat pipe expands the range of applications of heat pipes especially in thermal management applications. Flat heat pipes have been applied mainly in electrical and electronic devices cooling. *Ye* et al. [17] conducted an experimental study on a micro flat heat pipe array (MHPA) used to cool lithium-ion battery packs. The battery temperature during charging and discharging cycles was measured with and without utilising the heat pipe system. The results indicated that the temperature difference between the battery cells was uniform with less than a 6.5 °C difference by cooling the cells using the MHPA. In solar applications, a flat heat pipe increases the heat transfer area which is exposed to the solar radiation. Moreover combining flat heat pipes with photovoltaic modules increases the electrical efficiency of these hybrid systems and simplifies the structure for manufacturing and installation. *Jouhara* et al. [18] have investigated the performance of a flat heat pipe combined with a PV panel to harness heat and electricity from solar energy simultaneously. The flat heat pipe PV/T system exhibited a total efficiency of 56% and increased the efficiency of the

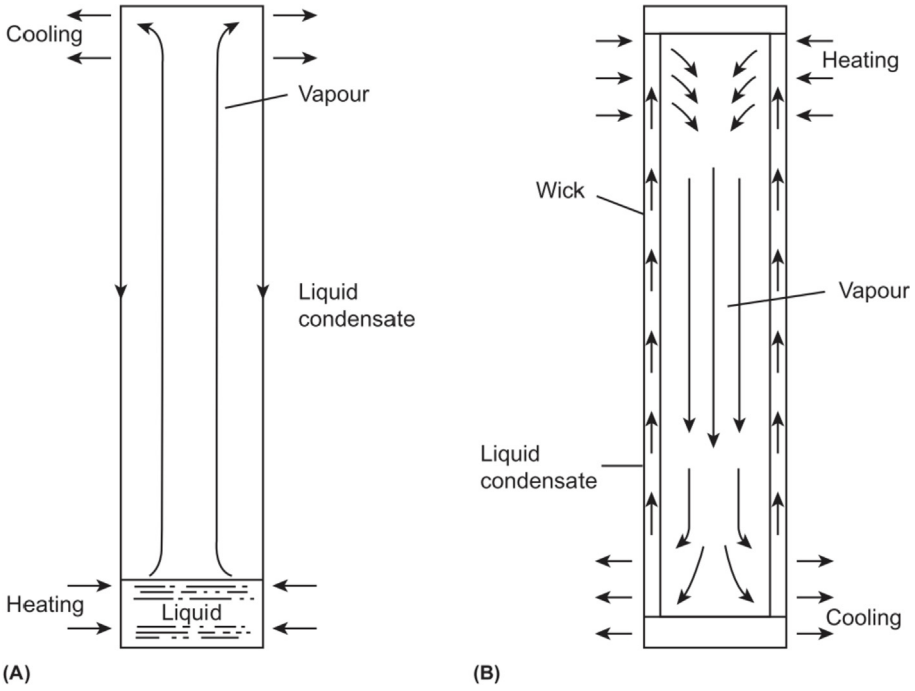

Fig. 1. Structure of heat pipes: (A) thermosyphons, (B) wicked heat pipes [11].

PV panel by 15% because of the cooling by the flat heat pipe. The flat heat pipe [19] is an innovative technology which can recover heat by radiation and forced convection from hot sources. Utilising such an effective heat recovery technology can reduce the energy consumption in steel manufacture and reduce total production costs. The flat heat pipe is different from what was presented in the literature in [16]. The FHP in this paper is designed to operate at different inclination angles starting from a vertical position to a nearly horizontal position. The presented FHP in this research cannot operate in a horizontal position as the heat pipe in [16] because the working fluid does not return to the evaporator at the horizontal position. In the earlier investigation [19], the FHP was tested in the laboratory and in a factory for heat recovery by thermal radiation. In the laboratory the FHP was exposed to an electrical heater to simulate the hot steel. The FHP was tested at heater temperatures of 500 °C and 580 °C and two tests were carried on in the factory application. In this investigation the FHP was tested at different heater temperatures in the laboratory with different setups of the FHP. The multiple vertical pipes of the FHP increases the maximum heat transfer capability of the heat pipe at high fluxes.

The thermal radiation absorptivity of the FHP surface can be enhanced by applying a coating that maximises the absorptivity at a certain wave length and which can withstand high temperatures in a harsh environment. Many investigations have been carried out on selective coatings for solar collectors which capture heat at the wave length range of visible light. *Abbas* [20] carried out an investigation on the performance of three solar collectors with different coatings. The investigation concluded that the selective coating increased the efficiency of the system by 30% in comparison to a black paint coating. The main aspects for selecting and developing selective coatings are the thermal and chemical stability at the temperature of the coated surface, the optical properties in terms of having a high spectral absorptivity and low emissivity, good resistance to the environment conditions and cost-effectiveness.

The performance of radiative heat exchangers and collectors can also be enhanced by attaching fins to the tubes which increase the heat transfer area. Radiation heat transfer between the fins and the heat source or surroundings complicates the theoretical derivation of the fin efficiency. *Zhang* et al. [21] conducted a thermal analysis of a liquid metal heat pipe radiator for a space power reactor. The proposed system comprised a heat pipe system provided with integral fins covering the pipes. The performance of the heat pipe system was studied mathematically and numerically. The temperature distribution along the heat pipe radiator fins was compared with pumped loop radiator fins. The results revealed that the heat pipe fins have an isothermal characteristic in the direction of the heat pipe length.

In this piper, the effect of the radiation absorptivity and emissivity of the FHP surface in addition to the extended evaporator surface under radiation heat transfer condition is investigated experimentally and theoretically.

2. Experimental apparatus

The flat heat pipe consisted of 14 stainless steel tubes (28 mm OD) connected by a bottom collector (38 mm OD) and a shell and tube condenser top header. The heat transfer area was increased by attaching a stainless-steel sheet to the back of the tubes. This back panel acted as an extended surface as it absorbed radiation from the heat source and transferred it to the pipes by conduction and radiation. The mechanical design of the FHP is shown in Fig. 2.

Fig. 3 illustrates a 2D drawing of the FHP including the main dimensions. The overall dimensions of the FHP are 1 m by 1 m. The surface area exposed to the radiative heat is 0.675 m^2.

The experimental setup consisted of the FHP and electrical heater lamps that simulated the hot steel in the factory. The FHP was tested at different heater temperatures by varying the electrical input to the heaters. In addition, the effect of the FHP surface emissivity was examined by painting the FHP with high temperature black paint. The FHP was also tested with and without a back panel in order to evaluate the impact of the back panel on the heat recovery. The FHP was tested at different setups as follows: with a

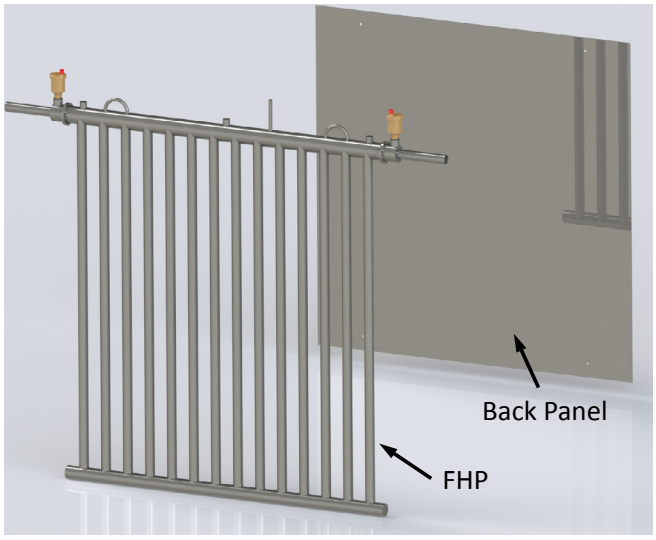

Fig. 2. FHP mechanical design.

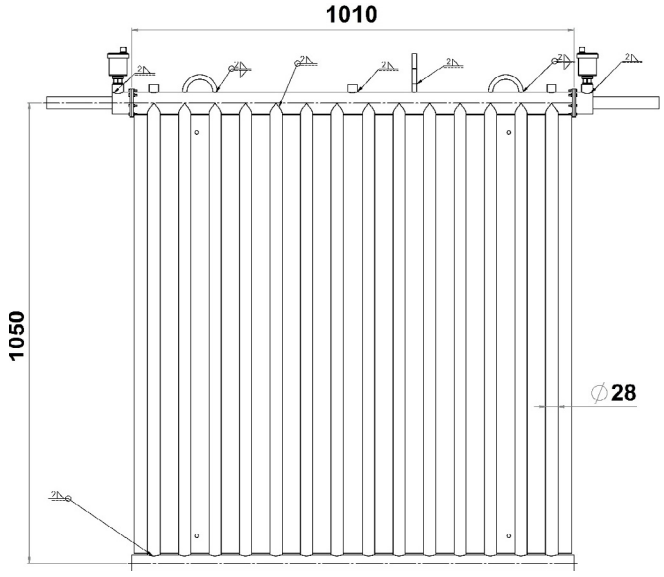

Fig. 3. 2D drawings of the FHP.

back panel and unpainted, without a back panel and unpainted, with a back panel and painted, without a back panel and painted.

The temperatures were measured using K-type thermocouples and national instruments data logging system, where the uncertainties associated with the temperature readings are (0.05% rdg ± 0.38 °C).

The thermocouples placed on the FHP are shown in Fig. 4 (a). The surface temperature of the FHP was measured by installing 2 thermocouples on the bottom collector (BC1-BC2), 9 thermocouples on the pipes of the FHP (HP1− HP9), and 2 on the top header to measure the working temperature of FHP, which corresponds to the adiabatic section (AD1- AD2). The water flow rate was measured using a turbine flow meter (Omega FTB 371 turbine flow sensor) where the uncertainty associated with the measurements is ±1% of the full scale. The rate at which heat was recovered was obtained by measuring the flow rate and the temperatures of the water inlet and water outlet.

The top header and the back panel were insulated using superwool thermal insulation. The FHP vertical pipes where uninsulated from the back when it was tested without a back panel. In order to evaluate of the impact of the back panel, the back panel was also uninsulated when it was painted and attached to the FHP in test 4.

The FHP was placed in front of electrical heater lamps which radiated heat to it. The experimental setup is presented in Fig. 4 (b), Fig. 5 (a), and Fig. 5 (b).

The experimental conditions of the tests are summarised in Table 1.

The electrical heaters emit the heat directly to the FHP and to the surroundings. In addition, they transfer by conduction to the support plate which emits the heat by radiation to the FHP and surroundings in turn. Table 2 presents the individual heater temperature and the average temperature of the heaters plate including the heaters.

3. Theoretical analysis

3.1. Theoretical modelling

The electrical heaters emitted heat by radiation to the FHP and by natural convection and radiation to the surroundings. The heat absorbed by the external evaporator wall of the FHP was conducted to the inner surface of the evaporator. Then the heat was transferred to the working fluid in the heat pipe by boiling and the working fluid vaporised, with the vapour flowing towards the condenser. The working fluid vapour condensed at the outer wall of the condenser tubes. The latent heat of condensation was transferred from the outer wall of the condenser to the inner surface of the condenser tubes by conduction and thence by forced convection heat transfer to the coolant. Finally, the condensate returned to the evaporator, assisted by gravitational forces. In order to predict the thermal performance of the FHP, which is essentially a thermosyphon, the heat transfer process is modelled via a series of thermal resistances and the analysis of the thermal network is performed using the electrical analogy approach. A schematic of the thermal network model is presented in Fig. 6.

The thermal resistances shown in Fig. 6 are:

R_{rad}: Radiation thermal resistance at the evaporator section
R_{cond_e}: Conduction thermal resistance of the evaporator wall
R_{ei}: Boiling thermal resistance
R_{ci}: Condensation thermal resistance
R_{cond_c}: Conduction thermal resistance of the condenser wall
R_{co}: Convection thermal resistance of condenser section

The thermal resistance due to the vapour flow from the evaporator to the condenser is negligible in comparison to the other thermal resistance. Therefore it was not considered in the theoretical modelling.

A theoretical modelling tool was build based on the thermal network model and the heat transfer analysis presented in this paper using correlation published in the literature.

3.2. Radiation analysis

The FHP absorbs radiation from the heaters, which radiate in all directions. The view factor between the heaters and the FHP has to be determined, in order to calculate the heat radiated towards the FHP. The assembly of the FHP with the back panel results in a complex geometry for the radiation modelling. It was assumed that the flat heat pipe with the back panel acts as a flat surface to simplify the geometry. Radiation to the FHP surface is represented by the heat received by the highlighted plane (FHP), while the

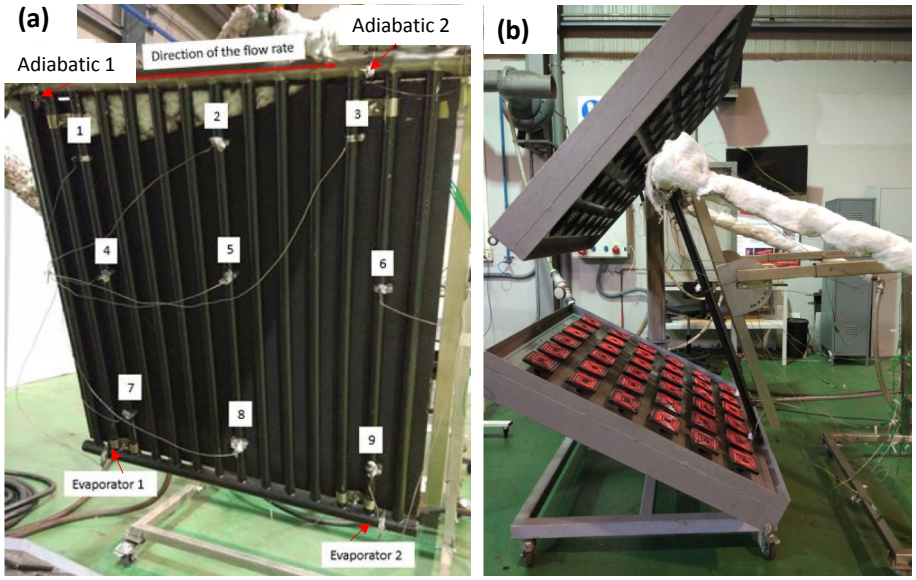

Fig. 4. FHP Experimental setup.

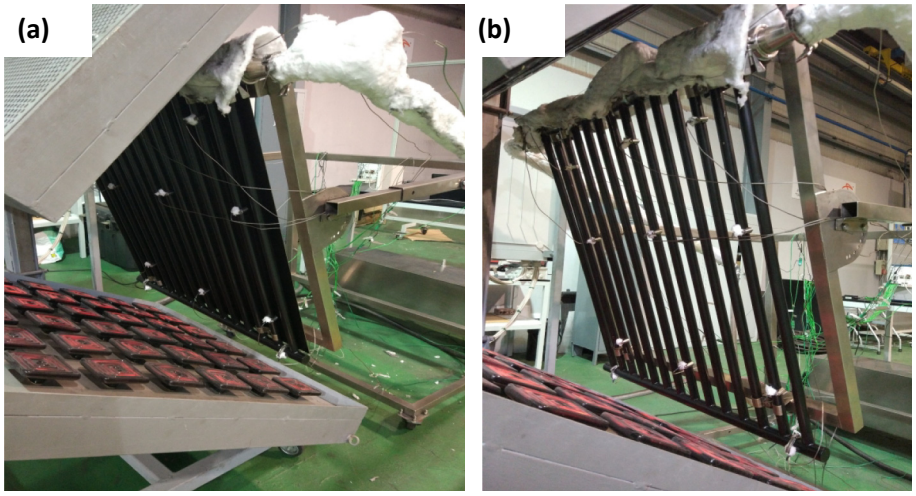

Fig. 5. (a) FHP testing with black paint and back panel, (b) FHP testing without a back panel and with black paint.

Table 1
Experimental conditions of the FHP tests.

Test Number	Test condition	Water flow rate	Water inlet temperature	Heater temperature	Maximum water outlet temperature	Maximum Heat recovery	Heat Flux
		(L/min)	(°C)	(°C)	(°C)	(kW)	(W/m^2)
Test 1	No Back panel/No paint	15	18.9	400–580	20.4	1.4	2072
Test 2	Back panel/No paint	25	10.6	400–580	14.2	5.8	8587
Test 3	No Back panel/Black paint	15	21.4	400–580	28.3	7	10363
Test 4	Back panel/Black paint	18	21	400–580	28	8.5	12584

Table 2
Heaters temperature and average temperatures of the overall heaters plate.

Heater temperature	Average temperature of the heating plate
400	397
470	427
500	489
580	544

heater plate surface is represented by plane (H) as shown in Fig. 7 (a).

In Fig. 7 (b) the heaters plate surface is represented by dimension (H), while the FHP surface is represented by dimension (FHP). The view factor between (H) and (FHP) can be obtained by following the view factor algebra approach. By applying the superposition rule, and reciprocity rule in radiation heat transfer:

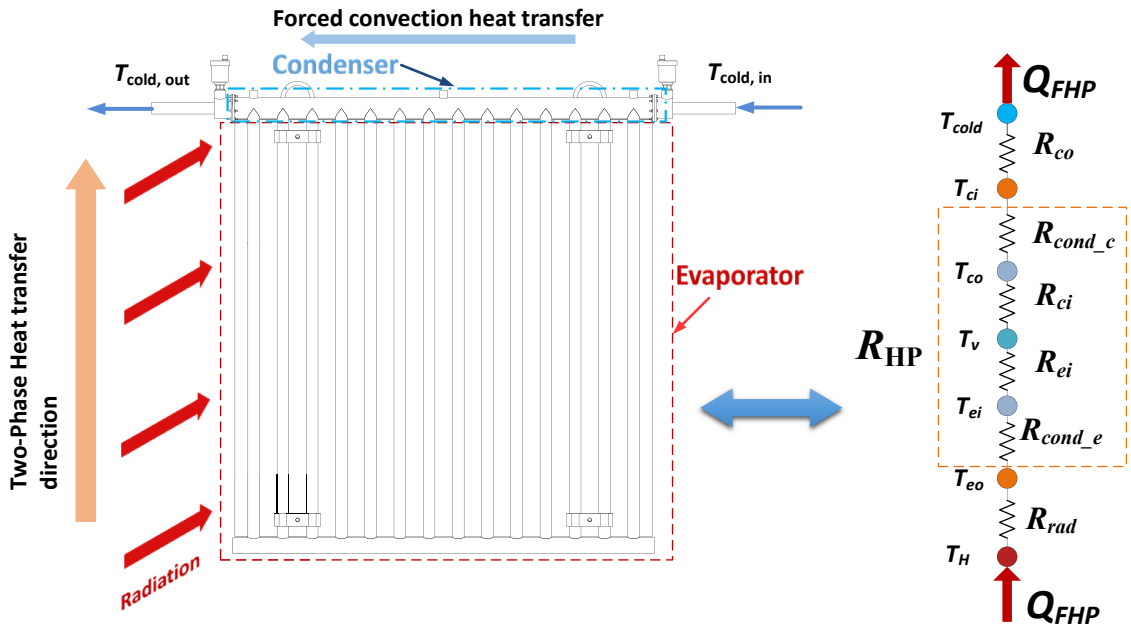

Fig. 6. Schematic of the thermal network modelling of the FHP.

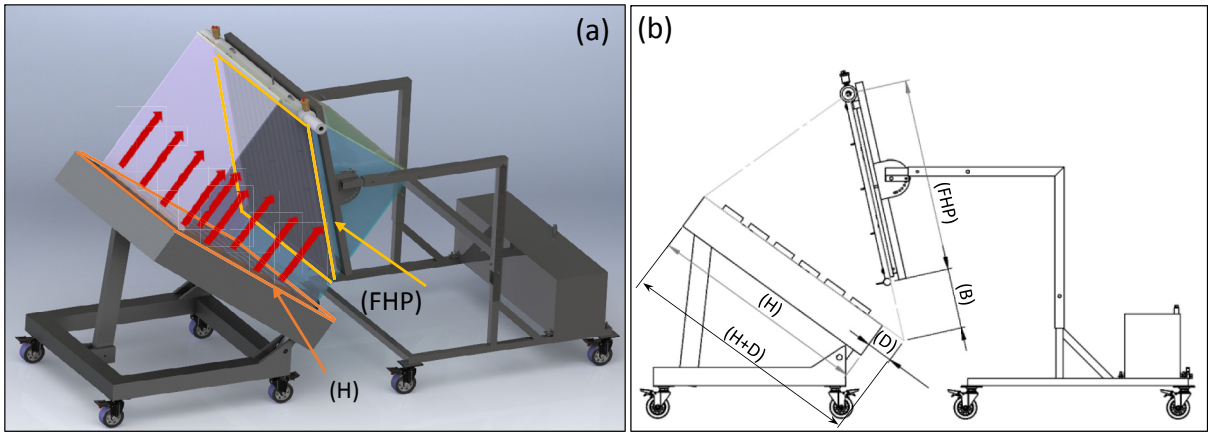

Fig. 7. Planes nomenclature used in view factor determination.

$$F_{H\to FHP} = \frac{1}{A_{(H)}}\left(A_{(H,D)}F_{(H+D)\to(FHP+B)} - A_D F_{D\to(FHP+B)} - A_{(H+D)}F_{(H+D)\to B} + A_D F_{D\to B}\right) \quad (1)$$

where $A_{(H)}$ is the surface area of heaters plate.where the view factors values are calculated using a catalogue of radiation heat transfer configuration factors [22]:

$$F_{(H+D)\to(FHP+B)} = 0.5,\ F_{D\to(FHP+B)} = 0.782, F_{(H+D)\to B} = 0.188,\ F_{D\to B} = 0.689 \quad (2)$$

Hence the view factor between the heaters plate and the FHP with the back panel attached:

$$F_{H\to FHP} = 0.361 \quad (3)$$

The view factor between the heaters plate and the FHP without a back panel is calculated by applying the following analytical approach. The radiative heat from the heaters to the FHP with a back panel consists of the radiative heat from the heaters plate incident on the FHP vertical pipes and the bottom collector, in addition to the radiative heat from the heaters plate to the spaces between the vertical pipes. As a result, the view factor between the heaters and the FHP without a back panel is obtained from the following:

$$F_{H\to FHP(no\ panel)} = F_{H\to FHP} - F_{H\to FHP(spaces)} \quad (4)$$

Hence:

$$F_{H\to FHP(no\ panel)} = 0.25 \quad (5)$$

Thermal modelling of heat transfer by radiation is presented in Fig. 8.

The modelling of the radiation heat transfer was based on assuming that all the surfaces act as grey and diffusive bodies.

The net heat transfer by radiation between the heaters and the FHP was obtained from the energy balance between the three bodies: the heaters, the FHP, and the surroundings.

Summing the currents at node 1 in Fig. 8 yields:

$$\frac{E_H - J_H}{\frac{1-\varepsilon_H}{\varepsilon_H A_H}} = \frac{J_H - J_{eo}}{\frac{1}{A_H F_{12}}} + \frac{J_H - E_{surr}}{\frac{1}{A_H F_{13}}} \quad (6)$$

Summing the currents at node 2 yields

$$\frac{E_{eo} - J_{eo}}{\frac{1-\varepsilon_{eo}}{\varepsilon_{eo} A_{eo}}} = \frac{J_{eo} - J_H}{\frac{1}{A_{eo} F_{21}}} + \frac{J_{eo} - E_{surr}}{\frac{1}{A_{eo} F_{23}}} \quad (7)$$

By solving equations (6) and (7), J_{eo} and J_H can be determined. Then the heat transfer by radiation can be calculated from:

$$Q_{FHP} = \frac{E_{eo} - J_{eo}}{\frac{1-\varepsilon_{eo}}{\varepsilon_{eo} A_{eo}}} \quad (8)$$

3.3. Two-phase analysis

The heat pipe consists of three sections; evaporator, adiabatic section, and condenser. Heat is transferred to and from the heat pipe at the evaporator and the condenser, respectively.

The working fluid boils at the evaporator, vaporises, and flows towards the condenser section. The heat transfer rate at the evaporator section is represented by:

$$Q_{ei} = \frac{T_{ei} - T_v}{R_{ei}} \quad (9)$$

where:

Q_{ei}: Heat transfer rate by boiling (W)
T_{ei}: Evaporator inner wall temperature (K)
T_v: Vapour temperature which is equal to the saturation temperature (K)
R_{ei}: Thermal resistance of heat transfer by boiling (K/W)

The thermal resistance of boiling can be calculated as follows:

$$R_{ei} = \frac{1}{h_{ei} A_{ei}} \quad (10)$$

A_{ei}: Evaporator inner surface area (m^2)

$$A_{ei} = \frac{\pi}{2} \times D_{ei} \times L_e \times N_{evaporator\ pipes} + \frac{\pi}{2} \times D_{b.\ collector} \times L_{b.\ collector} \quad (11)$$

h_{ei}: Boiling heat transfer coefficient (W/m^2. K)

The heat transfer coefficient for boiling can be determined using the Rohsenow correlation [23] which is widely used to determine nucleate boiling heat transfer

$$h_{ei} = \mu_l . h_{fg} \left[\frac{g.(\rho_l - \rho_v)}{\sigma}\right]^{\frac{1}{2}} . \left[\frac{c_p}{\left(C_{sf} . h_{fg} . \mathrm{Pr}_l^n\right)}\right]^3 . (T_{ei} - T_v)^2 \quad (12)$$

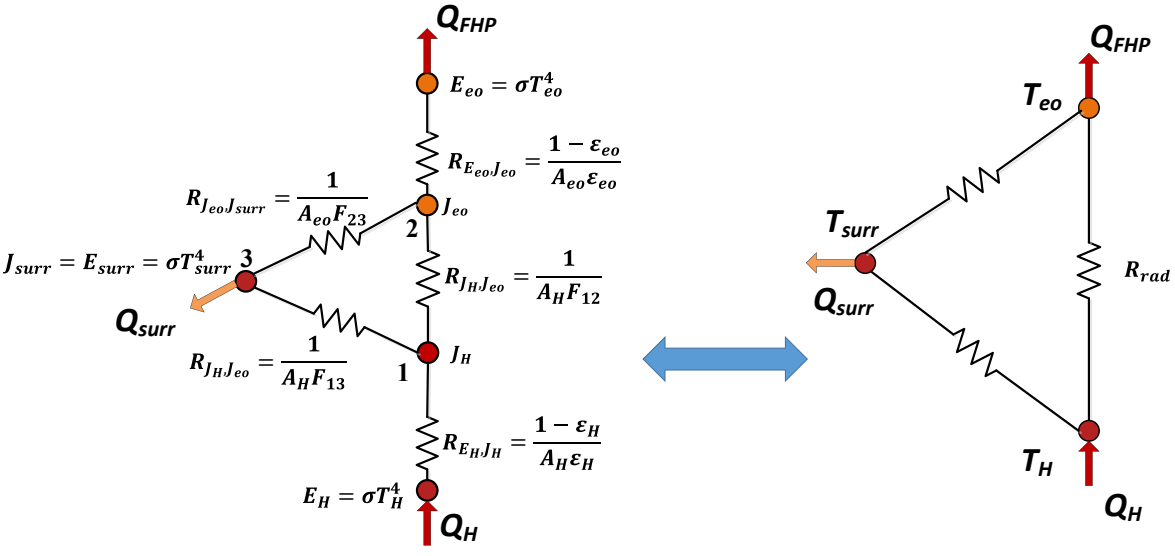

Fig. 8. Schematic of thermal radiation resistance modelling.

E_H: is the heat emitted from the heater surface (W/m^2)
E_{eo}: Heat emitted from the evaporator of the FHP surface (W/m^2)
E_{surr}: Heat emitted from the surroundings (W/m^2)
J_H: Radiosity of the heater surface which is the overall radiation leaving the heater surface (W/m^2)
J_{eo}: Radiosity of the evaporator surface which is the overall radiation leaving the evaporator surface (W/m^2)
J_{surr}: Radiosity of the surrounding (W/m^2)
$R_{E_H J_H}$: Heater surface resistance to radiation (m^{-2})
$R_{J_H J_{eo}}$: Space resistance to radiation between the heaters and the FHP (m^{-2})
$R_{E_{eo} J_{eo}}$: Evaporator surface resistance to radiation (m^{-2})
R_{rad}: Radiation heat transfer resistance (K/W)
F_{12}: View factor between node 1 and 2 which is the view factor between the heaters plate and external surface of the FHP ($F_{H \to FHP}$).
F_{13}: View factor between node 1 and 3 which is the view factor between the heaters plate and surrounding ($F_{H \to surr}$)
F_{21}: View factor between node 2 and 1 which is the view factor between external surface of the FHP and the heaters plate ($F_{FHP \to H}$)
F_{23}: View factor between node 2 and 3 which is the view factor between external surface of the FHP and surrounding ($F_{FHP \to surr}$)

At the condenser section, the vapour condenses rejecting the heat to the coolant through the condenser tubes walls. The heat transfer rate by condensation is represented as follows:

$$Q_{co} = \frac{(T_v - T_{co})}{R_{co}} \quad (13)$$

where.

Q_{co}: Heat transfer rate by condensation (W)
T_v: Vapour temperature (K)
T_{co}: Temperature of outer surface of the inner tubes
R_{co}: Thermal resistance of heat transfer by condensation

$$R_{co} = \frac{1}{h_{co}.A_{co}}$$

A_{co}: Heat pipe condenser area which represents the overall external surface area of the horizontal tubes in the condenser section (m^2).

$$A_{co} = \pi \times D_{co} \times L_c \times N_{water\ tube} \quad (14)$$

D_{co}: Condenser outer diameter (m)
L_c: Condenser length (m)
$N_{water\ tube}$: Number of water tubes
h_{co}: Condensation heat transfer coefficient (W/m^2. K)

The condensation heat transfer coefficient can be calculated by using the Nusselt correlation [24].

$$h_{co} = 0.725\left[\frac{\rho_l(\rho_l - \rho_v)gh^*_{fg}k_l^3}{D_{co}\mu_l(T_v - T_{co})}\right]^{\frac{1}{4}} \times \frac{1}{N^{1/4}_{tube\ rows}} \quad (15)$$

where h^*_{fg} is the modified latent heat of vaporisation which is calculated by the following formula [25].

$$h^*_{fg} = h_{fg} + 0.68C_p(T_v - T_{co}) \quad (16)$$

$N_{tube\ rows}$ is the number of rows of tubes where the condensate drops from the top tube to the tube below it.

Fig. 9 (A) shows a three-dimensional view of the FHP. Fig. 9 (B) illustrates a sectional view of the FHP condenser section. It can be seen that condensate drops from the top tube to the outer surface of the tube below because of the gravitational force and flows back to the evaporator. The liquid dropping from the upper tubes increases the condensate film on the lower tubes decreasing the overall heat transfer coefficient.

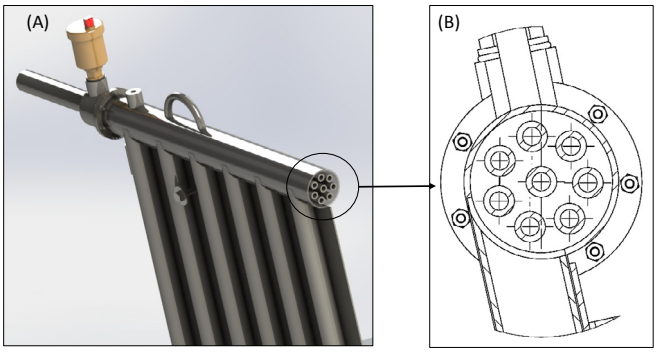

Figure 9. (A) 3D section view of the FHP. (B) Section view of the FHP condenser.

3.4. Forced convection heat transfer

The heat transferred by forced convection from the inner surface of the condenser tubes to the water. The heat transfer rate is expressed as follows:

$$Q_{co} = h_{ci}.A_{ci}.LMTD = \frac{LMTD}{R_{ci}} \quad (17)$$

where:

LMTD is the logarithmic mean temperature of the cooling fluid (K):

$$LMTD = \left(\frac{(T_{ci} - T_{cold,\ in}) - (T_{ci} - T_{cold,out})}{\ln\left(\frac{T_{ci}-T_{cold,out}}{T_{ci}-T_{cold,\ in}}\right)}\right) \quad (18)$$

h_{ci}: Heat transfer coefficient of forced convection (W/m^2. K).

The forced convection heat transfer coefficient is calculated by using the Gnielinski correlation [26]:

$$Nu = \frac{(f/8)(Re - 1000)Pr}{1 + 12.7(f/8)^{1/2}(Pr^{2/3} - 1)}\left[1 + (D_{ci}/L_c)^{2/3}\right]\left(\frac{Pr}{Pr_{ci}}\right)^{0.11} \quad (19)$$

3.5. This correlation is applicable for the Reynolds number range $2300 < Re < 5 \times 10^6$

where f is a friction factor calculate d from the following correlation:

$$f = (1.82\log_{10}Re - 1.64)^{-2} \quad (20)$$

3.6. Conduction heat transfer

The heat transfer by conduction at the evaporator is given as follows:

$$Q = \frac{T_{eo} - T_{ei}}{R_{cond,e}} \quad (21)$$

$R_{cond,e}$: The thermal resistance of evaporator wall conductivity is given as follows:

$$R_{cond,e} = \frac{\ln(D_{eo}/D_{ei})}{\pi l_e k_s N_{evaporator\ pipes}} \quad (22)$$

D_{eo}: Outer diameter of the evaporator pipes (m)
D_{ei}: Inner diameter of the evaporator pipes (m)
l_e: Length of the evaporator pipes
k_s: Thermal conductivity of evaporator wall (W/m.K)

In a similar way, the heat transfer by conduction at the condenser and the thermal resistance of the wall of the condenser are given as follows:

$$Q = \frac{T_{co} - T_{ci}}{R_{cond,c}} \tag{23}$$

$$R_{cond,c} = \frac{\ln(D_{co}/D_{ci})}{2\pi l_c k_s N_{water\ tube}} \tag{24}$$

D_{co}: Outer diameter of the condenser tubes (m)
D_{ci}: Inner diameter of the condenser tubes (m)
l_c: Length of the condenser tubes
k_s: Thermal conductivity of condense wall (W/m.K)
$N_{water\ tube}$: Number of water tubes in the condenser

The heat transfer rate in the condenser section can be calculated from the following equation also:

$$Q_{FHP} = \dot{m}.C_p.(T_{cold,out} - T_{cold,in}) \tag{25}$$

By solving the equations for the heat transfer rate together, considering energy conservation, the net heat transfer rate through the heat pipe can be obtained.

4. Results and discussion

4.1. Experimental results

4.1.1. Effect of heater temperatures

The results from tests on the FHP are shown in Fig. 10. It can be noted that the heat recovery increased with increasing heater temperature. The gradients of the curves for heat recovery are, in general, consistent with the increase in electrical heater input. The magnitude of the rate of heat recovery varied between 0.4 kW and 8.5 kW (2–12.7 kW/m^2 of heat flux per evaporator surface area) during the tests. Moreover, it can be seen from Fig. 10 that the amount of heat recovery for the FHP unpainted and without a back panel was very low and the effect of the heater temperature on the performance of the FHP was insignificant. This was due to the fact that the FHP was exposed to an inadequate heat flux, since the back panel was removed and most of the incident radiation on the FHP surface was reflected. It can be seen also that the best thermal performance and highest amount of heat transfer rate was achieved when the FHP was assembled with the back panel and painted black.

4.1.2. Effect of the back panel

The effect of the back panel on the FHP thermal performance is presented in Fig. 11 for two cases: when the FHP was not painted and with it painted black. In the case when the FHP was not painted, the amount of heat recovery significantly increased when compared to the test without a panel. This can be explained by the fact that the back panel acted as an extended surface, which increased the heat transfer area of the FHP. The back panel absorbed thermal radiation and transferred it to the pipes by conduction. In addition, the back panel emitted and reflected radiative heat, where a fraction of this heat was absorbed by the pipes. In the case of an unpainted FHP the improvement in heat recovery increased from 175% at a heater temperature of 400 °C to 330% at a heater temperature of 580 °C. It can also be noted that, in this case, the efficiency of the back panel increased with the increment of the temperature. In contrast, the effect of the back panel on the painted FHP varied only between 11% and 31%. The impact of the back panel in the case of the unpainted FHP was greater than for the black painted FHP case because in the former case the back panel was insulated, which reduced heat losses by natural convection and radiation to the surroundings. The insulated unpainted back panel lost the heat from one side, while the black panel lost heat from both sides, the front and the back. The efficiency of the black back panel would be enhanced by adding insulation on the back side of it.

4.1.3. Effect of the black paint

The effect of the black paint on the thermal performance of the FHP is discussed for two cases as well: when the back panel was detached from the FHP, and when it was assembled as shown in Fig. 12.

The influence of the black paint on the heat transfer rate varied between 360% and 470% in the case of FHP without a back panel and it can be seen that the heat recovery enhancement appeared to decrease with increasing heater temperature. The unpainted FHP was unable to operate without a back panel at low heater temperatures, which shows the impact of the black paint on the performance. It can be understood that the incident radiation was reflected on the unpainted FHP pipes surface and the FHP was uninsulated from the back, which increased the heat loss by natural convection. By increasing the heater temperatures, the unpainted FHP started to operate under geyser boiling condition. However, the increment in the thermal performance of the unpainted FHP was less than for the case of the black painted FHP, indicating an

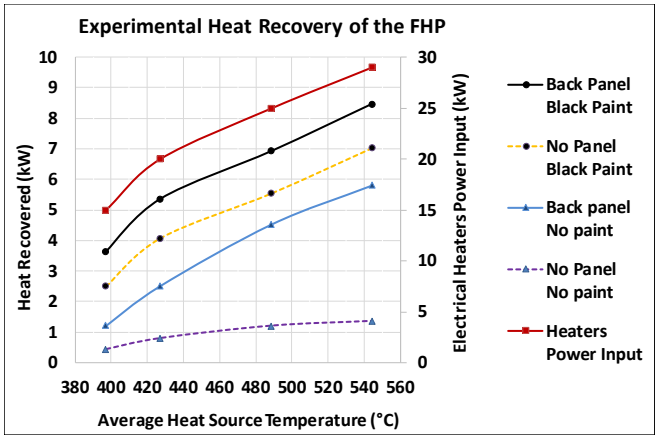

Fig. 10. Heat recovery by FHP at different heater temperature and conditions.

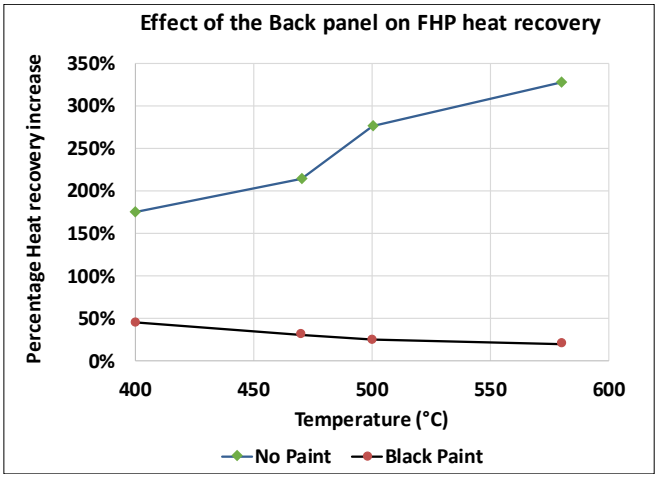

Fig. 11. Effect of the back panel on the amount of heat recovery.

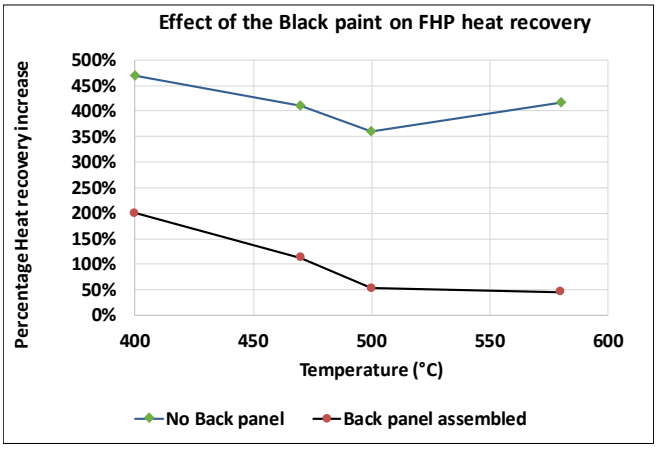

Fig. 12. Effect of the black paint on the amount of heat recovery.

increasing the impact of the paint.

In the case of the FHP assembled with the back panel the enhancement due to the black paint varied between 46% and 200%.The impact of the black paint decreased with the increased hot source temperature due to the following reasons. At heaters plate temperature of 400 °C and 488 °C, the FHP with a back panel was also working with presences of the geyser boiling. The increase of the heater temperature increased the amount of heat recovery but also increased the surface temperature of the FHP and the back panel. As a result, heat losses to the surroundings increased and heat losses by radiation started to play a significant role. Since the black painted back panel was uninsulated, increasing heat losses decreased the overall gain due to the black paint.

By comparing the impact of the back panel with the impact of the black paint at heaters temperature higher than 500 °C when the FHP was operating properly, it can be noted that the black paint has more impact than the back panel.

It is noted that the best case was when the FHP was assembled with the back panel and painted with black paint. Therefore, the results of this case are presented in Fig. 13 and Fig. 14.

The temperatures of the FHP during the test with black paint and back panel at heaters temperature is presented in Fig. 13. The temperature of the bottom collector was 73 °C and the average temperature readings of the 9 thermocouples on the vertical pipes was 68.4 °C. The average temperature of the adiabatic section was 52.6 °C. The temperature of the water inlet was 21 °C, and the temperature of the water outlet was 27.9 °C.

The amount of heat recovery is presented in Fig. 14. The heat transfer rate ranged between 7.9 kW and 9.4 kW with an average value of 8.5 kW. The fluctuation in the results was caused by the high mass flow rate of the water in comparison to the temperature difference between the inlet and outlet of the water. Where a fluctuation of 0.5 °C of the water temperature difference between the inlet and the outlet results in a 700 W of heat recovery difference at water flow rate of 18 l/min.

4.2. Theoretical results

The theoretical predictions based on the model presented previously are compared against the experimental results for the four cases of the tests. The theoretical results versus experimental results for heat recovery in the case of the FHP with no panel and unpainted are shown in Fig. 15. It can be observed that the theoretical heat recovery increases with increasing heat source temperature and the difference between the experimental results and the predictions was higher at higher heat source temperatures. The FHP was unable to function properly with the low heat fluxes for this arrangement, which could not be represented in the theoretical model.

The comparison of the results in the case of the FHP with black paint is presented in Fig. 16. It can be seen that the theoretical heat recovery was less than the experiments when the overall heat recovery was more than 3 kW. The theoretical model does not consider heat recovery by natural convection which explains the variance between the experimental and theoretical results. At a heat source temperature of 390 °C, the heat flux corresponding to

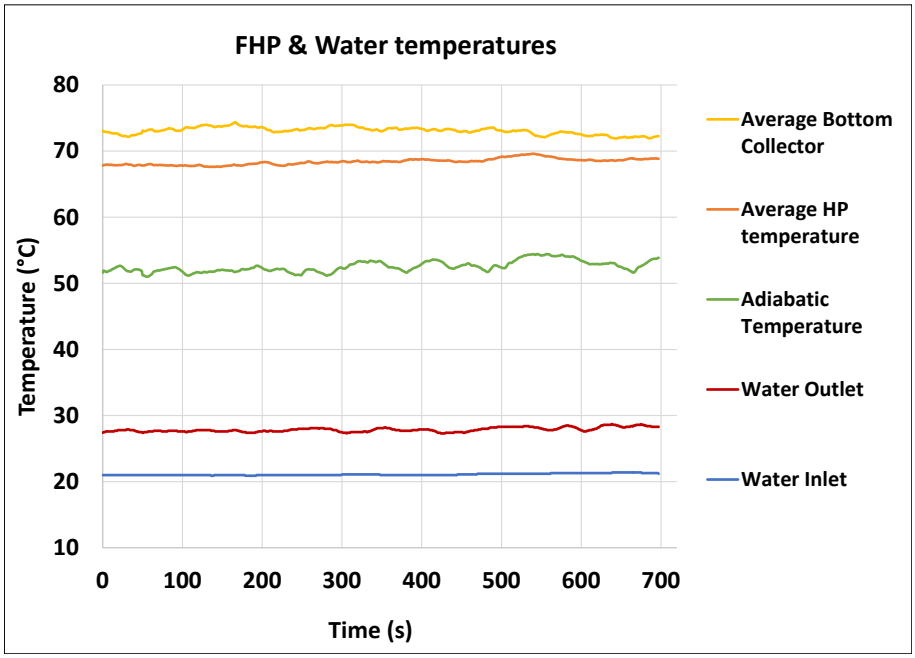

Fig. 13. FHP and water temperatures for FHP tests with a back panel and black paint at heater temperature 580 °C.

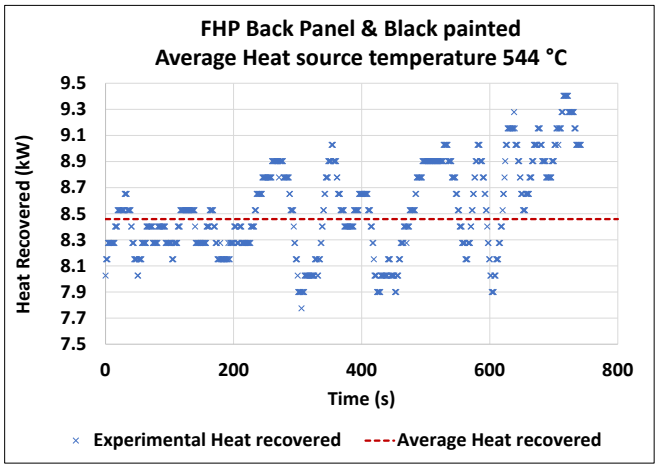

Fig. 14. Heat recovery by black painted FHP with a back panel at heater temperature 580 °C.

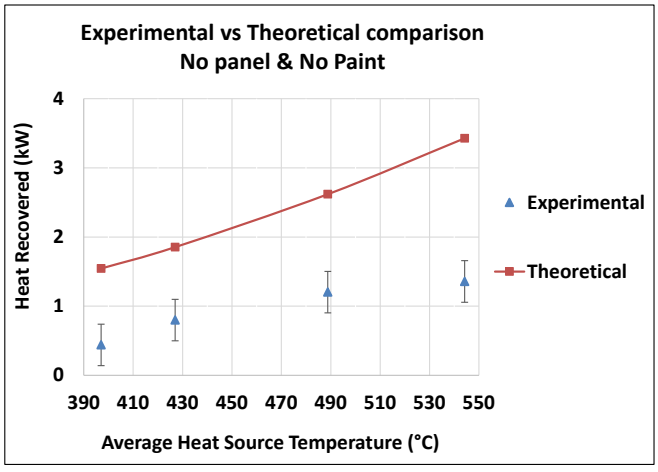

Fig. 15. Comparison between experimental and theoretical prediction of the heat recovery in the case no panel and no paint.

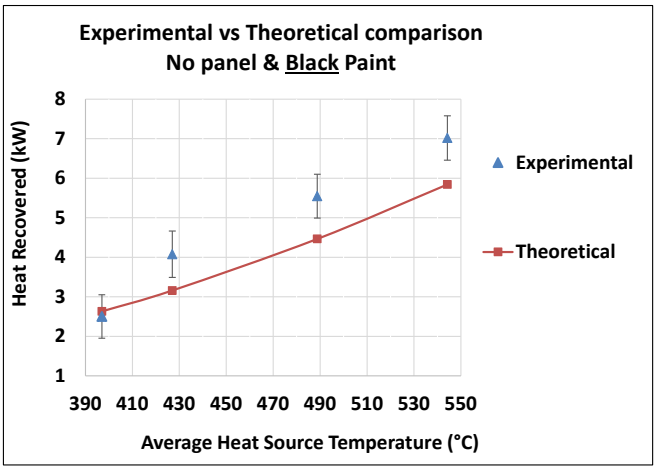

Fig. 16. Comparison between experimental and theoretical prediction of the heat recovery in the case no panel and black paint.

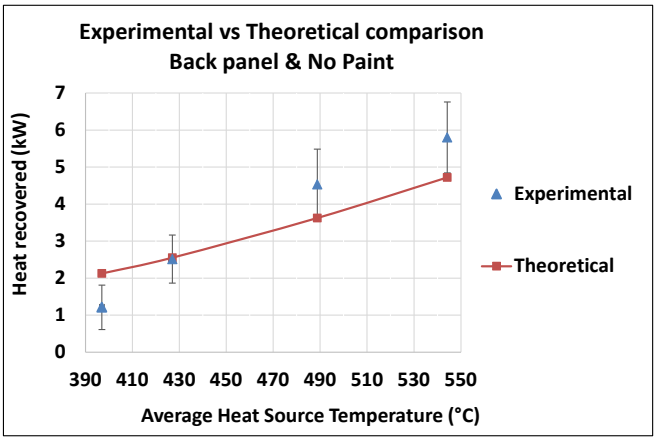

Fig. 17. Comparison between experimental and theoretical prediction of the heat recovery in the case back panel and black paint.

the heat source temperature and the hot air temperature was under the required value which enables the FHP to function ideally.

Fig. 17 presents the results obtained from testing the unpainted FHP with back panel. It can be seen that the theoretical heat recovery at a heat source temperature of 390 °C was higher than the experimental results while it was less than the experimental results for higher heat source temperatures.

Fig. 18 presents a comparison between the experimental and theoretical results for the case of the FHP with back panel and painted black. It can be noted that the experimental result was less than the prediction for the heat source temperature of 390 °c, while the experimental results became higher than the predictions when the heat source temperature increased and the FHP was operating at an ideal performance. It can be also observed that the difference between the experimental results and the prediction decreases by increasing the heat source temperature since the radiation starts to play a significant role in comparison to natural convection.

The experimental and theoretical results obtained from all the tests are compared in Fig. 19. It can be seen from the figure that most of the predictions lie within a ± 25% error. It can be seen also that when the FHP heat recovery is less than 3 kW, the error in the predictions exceeds 25%. This can be explained that the FHP functionality was not ideal as geyser boiling occurred in the heat pipe, which happens in heat pipes with low heat fluxes at the evaporator. When the temperature of the heaters was increased, the heat flux increased which enhanced the performance of the heat pipe. It can be seen that the theoretical results are under-predicted within 25%

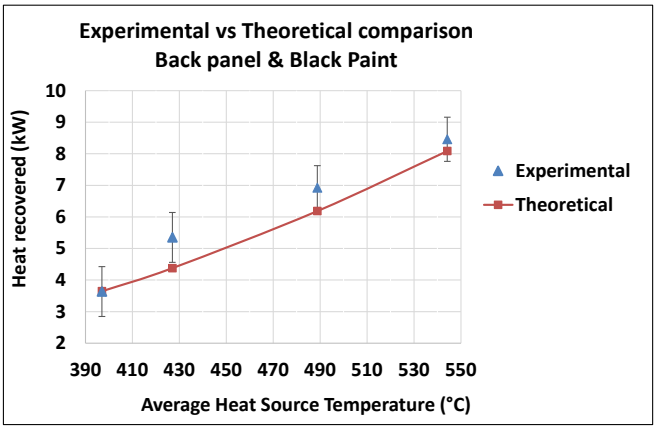

Fig. 18. Comparison between experimental and theoretical prediction of the heat recovery in the case back panel and no paint.

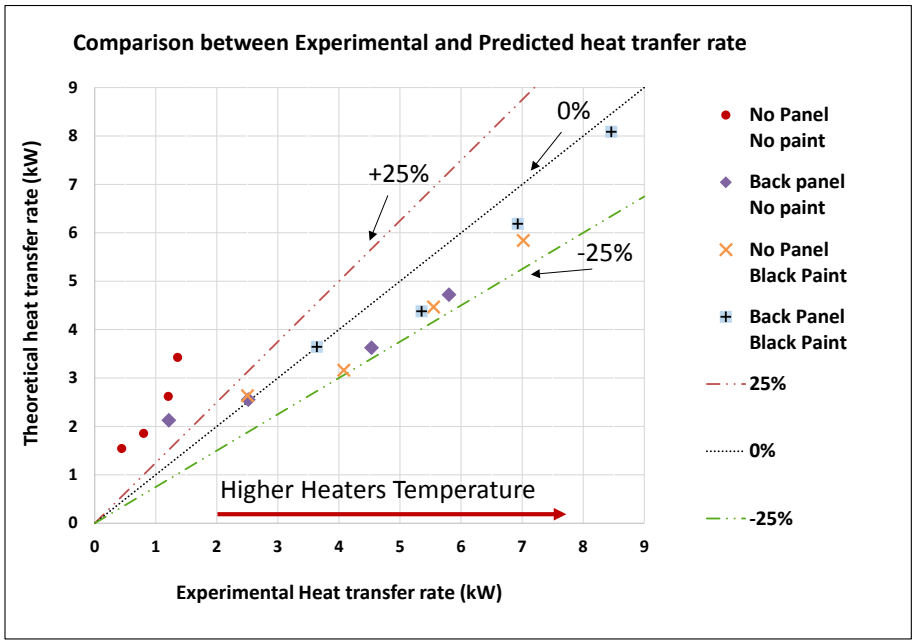

Fig. 19. Comparison between the experimental heat recovery of the FHP and the theoretical predictions.

Table 3
Maximum error associated with the experimental results.

Heat transfer rate (W)	Maximum error, S_Q	Maximum error S_Q/Q (%)
4532	±955	21.07%
5801	±956	16.49%
2502	±477	19.05%
4078	±530	13.00%
5548	±555	10.00%
7019	±576	8.21%
3637	±804	22.09%
5353	±775	14.48%
6925	±695	10.04%
8459	±704	8.32%

for the other tests. The modelling tool does not account for natural convection, while the FHP absorbs heat by radiation and natural convection in the real environment.

4.3. Uncertainties associated with the experimental results

The level of uncertainty for the experimental heat recovery values came from the temperature measurements, and the flow rate meter. The uncertainty associated the readings of the temperature is (0.05% ± 0.38), while the one associated with the flow meter is ±1% of the full scale.

According to [27], the propagation of uncertainties associated with the calculated heat transfer rate values (S_Q), can be calculated from:

$$S_Q = Q_{out} \times \sqrt{\left(\frac{S_{\dot{V}}}{\dot{V}}\right)^2 + \left(\frac{S_{(T_{water,out}-T_{water,in})}}{(T_{water,out}-T_{water,in})}\right)^2} \quad (26)$$

where the error associated with temperature difference between the water inlet and outlet is:

$$S_{(T_{water,out}-T_{water,in})} = \sqrt{S^2_{T_{water,out}} + S^2_{T_{water,in}}} \quad (27)$$

Uncertainty for the maximum heat transfer rate can be listed in the Table 3.

5. Conclusion

In this research, an experimental and theoretical investigation on a radiation-absorbing heat pipe heat exchanger was carried out to evaluate its thermal performance at different temperatures of a hot source. The radiant heat was emitted by electrical heaters that simulated a hot source of hot steel. The effect of the optical flat heat pipe surface characteristics represented by the FHP surface absorptivity and emissivity was investigated by testing the FHP with high temperature black paint. Moreover, the impact of increasing the radiation-absorbing heat transfer area was evaluated by testing the FHP with and without a back panel. It was observed that the black paint has a significant impact on the amount of heat recovered, increasing the heat transfer rate by up to 470%. Furthermore the back panel increased the heat transfer rate by up to 330%. The increase in the amount of heat recovery due to the black paint and the back panel together reached 570%, enabling the FHP to recover 8.5 kW.

The theoretical modelling tool was built to predict the thermal performance of the FHP. The thermal network model of the FHP system was presented and analysed. The theoretical predictions have a good agreement with the experimental results with less than 25% error.

The variation between the experimental and theoretical results was due to simplifying the complex geometry of the FHP in radiation heat transfer. In addition the theoretical modelling tool accounted for the radiation heat transfer gain without considering the natural heat exchanger with the ambience.

The accuracy of the modelling tool of the FHP system can be enhanced in the future work by considering the natural convection heat transfer between the FHP and the ambient air. The prediction can be further developed by investigating into more recent correlations for two-phase and single phase heat transfer.

This paper is a further investigation on a novel heat pipe heat exchanger technology for heat recovery applications from infrared

radiative sources.

It can also be concluded from this study that the flat heat pipe is an efficient technology for waste heat recovery applications in the steel industry.

Acknowledgements

The research presented in this paper has received funding from the European Union's Horizon 2020 research and innovation programme under grant agreement No. 680599.

References

[1] Olabi AG. 100% sustainable energy. Energy 2014;77:1–5. https://doi.org/10.1016/j.energy.2014.10.083.
[2] Olabi AG. Renewable energy and energy storage systems. Energy 2017;136:1–6. https://doi.org/10.1016/j.energy.2017.07.054.
[3] Jouhara H, Olabi AG. Editorial : industrial waste heat recovery. Energy 2018;160:1–2. https://doi.org/10.1016/j.energy.2018.07.013.
[4] Jouhara H, Khordehgah N, Almahmoud S, Delpech B, Chauhan A, Tassou SA. Waste heat recovery technologies and applications. Therm Sci Eng Prog 2018;6. https://doi.org/10.1016/j.tsep.2018.04.017.
[5] Zhang H, Wang H, Zhu X, Qiu YJ, Li K, Chen R, et al. A review of waste heat recovery technologies towards molten slag in steel industry. Appl Energy 2013;112:956–66. https://doi.org/10.1016/j.apenergy.2013.02.019.
[6] Liu J, Yu Q, Peng J, Hu X, Duan W. Thermal energy recovery from high-temperature blast furnace slag particles. Int Commun Heat Mass Transf 2015;69:23–8. https://doi.org/10.1016/j.icheatmasstransfer.2015.10.013.
[7] Gutiérrez Trashorras AJ, Álvarez EÁ, Río González JL, Suarez Cuesta JM, Bernat JX. Design and evaluation of a heat recuperator for steel slags. Appl Therm Eng 2013;56:11–7. https://doi.org/10.1016/j.applthermaleng.2013.03.019.
[8] Du WJ, Yin Q, Cheng L. Experiments on novel heat recovery systems on rotary kilns. Appl Therm Eng 2018;139:535–41. https://doi.org/10.1016/j.applthermaleng.2018.04.125.
[9] Ma H, Du N, Zhang Z, Lyu F, Deng N, Li C, et al. Assessment of the optimum operation conditions on a heat pipe heat exchanger for waste heat recovery in steel industry. Renew Sustain Energy Rev 2017;79:50–60. https://doi.org/10.1016/j.rser.2017.04.122.
[10] Jouhara H. 4.3 Heat pipes. Compr. Energy syst. Elsevier Inc; 2018. p. 70–97. https://doi.org/10.1016/B978-0-12-809597-3.00403-X.
[11] Reay D, Kew P. Heat pipes. 2006.
[12] Jouhara H, Chauhan A, Nannou T, Almahmoud S, Delpech B, Wrobel LC. Heat pipe based systems - advances and applications. Energy 2017;128:729–54. https://doi.org/10.1016/j.energy.2017.04.028.
[13] Jouhara H, Meskimmon R. An investigation into the use of water as a working fluid in wraparound loop heat pipe heat exchanger for applications in energy efficient HVAC systems. Energy 2018;156:597–605. https://doi.org/10.1016/J.ENERGY.2018.05.134.
[14] Jouhara H, Meskimmon R. Experimental investigation of wraparound loop heat pipe heat exchanger used in energy efficient air handling units. Energy 2010;35:4592–9. https://doi.org/10.1016/j.energy.2010.03.056.
[15] Delpech B, Milani M, Montorsi L, Boscardin D, Chauhan A, Almahmoud S, et al. Energy efficiency enhancement and waste heat recovery in industrial processes by means of the heat pipe technology: case of the ceramic industry. Energy 2018;158:656–65. https://doi.org/10.1016/j.energy.2018.06.041.
[16] Delpech B, Axcell B, Jouhara H. Experimental investigation of a radiative heat pipe for waste heat recovery in a ceramics kiln. Energy 2018. https://doi.org/10.1016/j.energy.2018.12.133.
[17] Ye X, Zhao Y, Quan Z. Experimental study on heat dissipation for lithium-ion battery based on micro heat pipe array (MHPA). Appl Therm Eng 2018;130:74–82. https://doi.org/10.1016/j.applthermaleng.2017.10.141.
[18] Jouhara H, Milko J, Danielewicz J, Sayegh M a, Szulgowska-Zgrzywa M, Ramos JB, et al. The performance of a novel flat heat pipe based thermal and PV/T (photovoltaic and thermal systems) solar collector that can be used as an energy-active building envelope material. Energy 2015:1–7. https://doi.org/10.1016/j.energy.2015.07.063.
[19] Jouhara H, Almahmoud S, Chauhan A, Delpech B, Bianchi G, Tassou SA, et al. xperimental and theoretical investigation of a fl at heat pipe heat exchanger for waste heat recovery in the steel industry. E, vol. 141; 2017. p. 1928–39. https://doi.org/10.1016/j.energy.2017.10.142.
[20] Abbas A. Solchrome solar selective coatings - an effective way for solar water heaters globally. Renew Energy 2000;19:145–54. https://doi.org/10.1016/S0960-1481(99)00028-2.
[21] Zhang W, Wang C, Chen R, Tian W, Qiu S, Su GH. Preliminary design and thermal analysis of a liquid metal heat pipe radiator for TOPAZ-II power system. Ann Nucl Energy 2016;97:208–20. https://doi.org/10.1016/j.anucene.2016.07.007.
[22] Howell J R, Pinar Menguc M, Siegel R. A catalog of radiation heat transfer configuration factors. Therm. Radiat. heat Transf.. sixth ed. CRC Press; 2015.
[23] Rohsenow WM. A method of correlating heat transfer data for surface boiling of liquids. Cambridge, Mass: MIT Division of Industrial Cooporation; 1951. 1951.
[24] Nusselt W. Die Oberflachenkondesation des Wasserdamffes the surface condensation of water. Zetrschr Ver Deutch Ing 1916;60:541–6.
[25] Rohsenow WM. Heat transfer and temperature distribution in laminar film condensation. Trans Asme 1956;78:1645–8.
[26] Gnielinski V. New equations for heat and mass-transfer in turbulent pipe and channel flow. Int Chem Eng 1976;16:359–68.
[27] Taylor J. Introduction to error analysis, the study of uncertainties in physical measurements. 1997.